

# Empowering Multi-class Classification for Complex Functional Data with Simultaneous Feature Selection

Shuoyang Wang and Guanqun Cao\* and Yuan Huang

*Department of Bioinformatics and Biostatistics, University of Louisville, U.S.A.*

*e-mail: [shuoyang.wang@louisville.edu](mailto:shuoyang.wang@louisville.edu)*

*Department of Statistics and Probability, Michigan State University, U.S.A.*

*e-mail: [\\*caoquanq@msu.edu](mailto:*caoquanq@msu.edu)*

*Department of Biostatistics, Yale University, U.S.A.*

*e-mail: [yuan.huang@yale.edu](mailto:yuan.huang@yale.edu)*

**Abstract:** The opportunity to utilize complex functional data types for conducting classification tasks is emerging with the growing availability of imaging data. However, the tools capable of effectively managing imaging data are limited, let alone those that can further leverage other one-dimensional functional data. Inspired by the extensive data provided by the Alzheimer’s Disease Neuroimaging Initiative (ADNI), we introduce a novel classifier tailored for complex functional data. Each observation in this framework may be associated with numerous functional processes, varying in dimensions, such as curves and images. Each predictor is a random element in an infinite dimensional function space, and the number of functional predictors  $p$  can potentially be much greater than the sample size  $n$ . In this paper, we introduce a novel and scalable classifier termed functional BIC deep neural network. By adopting a sparse deep Rectified Linear Unit network architecture and incorporating the LassoNet algorithm, the proposed unified model performs feature selection and classification simultaneously, which is contrast to the existing functional data classifiers. The challenge arises from the complex inter-correlation structures among multiple functional processes, and at meanwhile without any assumptions on the distribution of these processes. Simulation study and real data application are carried out to demonstrate its favorable performance.

**Keywords and phrases:** Classification, Deep neural networks, Feature selection, Functional data analysis, Lasso, Multidimensional functional data.

## 1. Introduction

Data considered in functional data analysis (FDA) include curves and images, which are commonly viewed as infinite-dimensional random vectors in a function space. Compared with classical independent and identically distributed (i.i.d.) data, the key distinguishing feature of functional data is the presence of dependence and smoothness within each data curve. There has been a recent surge in applications of multivariate functional data analysis due to new developments in neuroimaging (e.g. fMRI and PET) and electroencephalogram (EEG). Conventionally, the functional data is a collection of independently and randomly

---

\*To whom correspondence should be addressed.

observed samples which are real-valued functions,  $\{X_i(\mathbf{s})\}_{i=1}^n$ , where  $\mathbf{s} \in \mathcal{S}$ , is defined on a compact interval  $\mathcal{S} \subset \mathbb{R}^d$ ,  $d \geq 1$ . When  $d = 1$ , it refers to classical 1D functional data, i.e., curve data. When  $d > 1$ , it refers to multi-dimensional functional data, such as 2D or 3D imaging data ( $d = 2, 3$ ).

Our motivating example stems from the Alzheimer’s Disease (AD) Neuroimaging dataset (<http://adni.loni.usc.edu>), which is a longitudinal multicenter study designed to develop clinical, imaging, genetic, and biochemical biomarkers for early detection and tracking of AD. Given the dataset’s multidimensional nature, particularly its incorporation of PET imaging data and biochemical biomarker curve data, there exists significant scientific interest in predicting the status of new patients, whether they belong to the AD group, early mild cognitive impairment (EMCI) group, or the control (CN) group. The data’s composition, featuring both imaging and curve data, lends itself naturally to FDA, which has emerged as a popular method for AD data analysis and classification [20, 21, 10]. Notably, this dataset’s functional representation allows for a deeper understanding of the disease’s progression and offers valuable insights into potential diagnostic markers. Furthermore, considering the potential correlations among the observed functional data, we posit that a novel functional classifier, capable of capturing these correlations while selecting significant functional features, would be immensely advantageous in this complex functional data setting. As such, an approach that can capture correlations among signals and identify key functional features essential for accurate classification is needed.

There has been rich literature on functional data classification with a scalar response and univariate functional predictors. The prevalent technique applied in functional classification is based on the density function, the regression model and distance function. [13] considered the generalized functional linear model for the sparse functional data, where the integral is estimated by the first  $J$  truncated FPCs. [8] considered the representation of functional observations using splines basis, and they applied multivariate linear discriminant analysis to the spline coefficients to construct the classifier. [5] proposed the functional centroid classifier, where the distance is constructed by the absolute difference of inner products. [2] explored the nearest neighbor classifier in infinite dimensional metric space, and argued that the weak convergence of nearest neighbor classifier holds only if the metric space is separable with some regular conditions. Current functional data classification approaches often assume that the functions are i.i.d., limiting their ability to classify subjects based on multiple observed functions that are expected to be correlated. Recently, efforts have been made for multivariate functional data classification. [3] proposed classifiers for both univariate and multivariate functional data by extending the depth-based scalar outlyingness to an outlyingness matrix. [12] considered partial least square classification method for multivariate functional data defined in different domains.

However, many existing methods struggle with complex functional data, which involve both curve data

(1D functional data) and imaging data (2D and 3D functional data). As a more powerful tool to characterize the complex functions, Deep neural network (DNN) methods are recently used for multi-dimensional functional data classification to represent the powerful and complex classifiers. In particular, [19] and [17] proposed an optimal DNNs classifier for both densely and sparsely observed multi-dimensional functional data. However, they remain challenging to understand the dependency among multiple complex functional data. This is either because their functional representations lack the flexibility to capture intricate features or because they are designed for either curve functional data only [19], or imaging data only [17]. For a more detailed discussion of the development of functional data classification, we refer to recent review papers such as [18].

To address the aforementioned challenges and accomplish the classification task outlined in the motivating example, we introduce a novel and scalable classifier termed functional BIC deep neural network (fB-DNN). This classifier seamlessly integrates feature selection and classification, leveraging recent advancements in deep neural networks (DNNs)-based classifiers [17, 16]. Our contribution extends beyond the work presented in [17] by conducting a comprehensive investigation into the application of DNN procedures on multivariate multi-dimensional functional data spanning various domains. We begin by extracting the functional principal component scores (FPCs) of the data functions and proceed to train a penalized DNN using these FPCs and their corresponding class memberships. To achieve this, we adopt a sparse deep Rectified Linear Unit (ReLU) network architecture and incorporate the LassoNet algorithm proposed by [9]. LassoNet, a neural network architecture combining Lasso regularization with deep learning techniques, is designed to perform feature selection for supervised learning. Despite its demonstrated effectiveness in sparse DNNs for cross-sectional high-dimensional data settings, its potential in the context of functional data classification remains under-explored. We adapt the LassoNet algorithm from [9] to suit the requirements of functional classification, while also incorporating a high-dimensional BIC criterion to address the tendency of the original LassoNet algorithm to retain redundant features based on our empirical observations. Additionally, we develop the universal approximation theory and establish global optimality for the proposed classifier under the complex multi-dimensional functional data setting. We have also developed the convergence rate of the proposed classifier to the Bayes error when the optimizer has been reached.

Despite the emphasized importance of feature selection in the functional data analysis (FDA) literature, limited research has been conducted on analyzing their impacts on functional data classification. In existing literature, the focus of feature selection applied to functional data primarily revolves around replacing each infinite-dimensional observation with a finite-dimensional vector. For instance, [1] employed variable selection to identify intervals of the functional inputs corresponding to local maxima of the distance-covariance function. Similarly, [23] proposed Gaussian process discriminant analysis, integrating variable selection

and classification by treating each 1D functional data as a high-dimensional input and selecting significant intervals.

The advantages of feature selection in functional data classification are manifold. Firstly, it enhances interpretability and reduces monitoring costs by considering fewer functional varieties capable of discriminating the behavior of functional data, as opposed to all functional covariates. This approach is particularly helpful in allocating significant variables or image slices in imaging data classification problems. Secondly, feature selection leads to improved classifier performance by mitigating the negative impact of correlations between features on classification rates. For instance, in ADNI data analysis, classification accuracy is compromised when all functional features (such as 2D imaging slices) are included, as detailed in Section 5. Thus, selective inclusion of features based on their discriminative power can be a valuable feature.

Compared with the existing studies, we have two significant contributions. First, the DNN architecture we propose is fundamentally different. In this work, we introduce a novel DNN class that incorporates residual layers and penalty functions specifically for functional data. This architecture allows for functional feature selection. In contrast, our previous work [16, 17] did not include residual layers or penalty functions. The inclusion of these components not only enhances the model's ability to perform classification and feature selection simultaneously but also presents additional computational challenges. Second, the functional data types analyzed are different. Our previous work [16, 17], as well as most existing studies, focused on either 1D or multi-dimensional functional data classification. However, motivated by the complex ADNI data, we have developed a classifier that can handle both 1D and multi-dimensional functional data.

This article is organized as follows. In Section 2, we demonstrate the proposed functional classifier and feature selection procedure. An implementation of the the proposed classifier is considered in Section 3. Simulation studies are conducted in Section 4. Section 5 gives the application to the motivating real data. The conclusion of our study is summarized in Section 6. Additional algorithms and simulation results are given in the Appendix.

## 2. Formulation of functional data classification

### 2.1. Model setup

Throughout the paper, we consider  $p$ -dimensional functional covariates  $\mathbf{X} = \{X_j(\mathbf{s}_j)\}_{j=1}^p$ . In general,  $X_j$ 's are random processes defined on various domains with different dimensions  $d_j$ . Without loss of generality, we assume  $\mathbf{s}_j \in [0, a_1] \times \cdots \times [0, a_{d_j}]$  and  $a_l > 0$ ,  $l = 1, \dots, d_j$ . Let  $K \geq 2$  be the number of classes, and the class label  $Y \in \{1, \dots, K\}$ . For the class  $k$ , we denote the prior  $\pi_k = \mathbb{P}(Y = k)$ , such that  $\sum_{k=1}^K \pi_k = 1$ . In addition, we define the inner product  $\langle \cdot, \cdot \rangle$ , such that for any domain  $\mathcal{S}$ ,  $\langle f, g \rangle = \int_{\mathcal{S}} f(\mathbf{s})g(\mathbf{s})d\mathbf{s}$ , where  $f, g \in L^2(\mathcal{S})$ .

Suppose we observe  $n$  i.i.d. functional training samples  $\{(\mathbf{X}_i, Y_i) : 1 \leq i \leq n\}$ , which are independent of  $\mathbf{X}$  to be classified. We are interested in grouping a newly observed set of functional covariates  $\mathbf{X}$  to one of the  $K$  classes given the training data. Notably, each  $X_j : [0, 1]^{d_j} \rightarrow \mathbb{R}$  is assumed to be in  $L^2([0, 1]^{d_j})$ , such that  $\mathbb{E}\langle X_j(\mathbf{s}_j), X_j(\mathbf{s}_j) \rangle < \infty$ . Given  $Y = k$ ,  $X_j(\mathbf{s}_j)$  presumably has some unknown mean function  $\mathbb{E}X_j(\mathbf{s}_j) = \mu_{j|k}(\mathbf{s}_j)$  and unknown covariance function

$$\Omega_{j|k}(\mathbf{s}_j, \mathbf{s}'_j) = \mathbb{E}[(X_j(\mathbf{s}_j) - \mu_{j|k}(\mathbf{s}_j))(X_j(\mathbf{s}'_j) - \mu_{j|k}(\mathbf{s}'_j))].$$

By Mercer's Theorem, one has

$$\Omega_{j|k}(\mathbf{s}_j, \mathbf{s}'_j) = \sum_{\ell=1}^{\infty} \lambda_{j|k,\ell} \phi_{j|k,\ell}(\mathbf{s}_j) \phi_{j|k,\ell}(\mathbf{s}'_j), \quad \mathbf{s}_j, \mathbf{s}'_j \in [0, 1]^{d_j}, \quad (2.1)$$

where  $\{\phi_{j|k,\ell}\}_{\ell \geq 1}$  are orthonormal basis functions of  $L^2([0, 1]^{d_j})$ , such that  $\langle \phi_{j|k,\ell}, \phi_{j|k,\ell'} \rangle = 0$  for  $\ell \neq \ell'$  and  $\langle \phi_{j|k,\ell}, \phi_{j|k,\ell} \rangle = 1$  otherwise, and we assume eigenvalues  $\lambda_{j|k,1} \geq \lambda_{j|k,2} \geq \dots > 0$ . For any  $X_j(\mathbf{s}_j)$  under the  $k$ -th class, write  $X_j(\mathbf{s}_j) = \sum_{\ell=1}^{\infty} \xi_{j,\ell} \phi_{j|k,\ell}(\mathbf{s}_j)$ , where  $\xi_{j,\ell}$ 's are pairwise uncorrelated random coefficients across  $\ell$ . This representation of  $X_j(\mathbf{s}_j)$  is due to a multidimensional Karhunen-Loéve expansion. According to [5, 6], the infinite-dimensional vector of FPCs  $\boldsymbol{\xi}_j = (\xi_{j,1}, \xi_{j,2}, \dots)^\top$  provides an equivalent representation of  $X_j$ , and we consider the functional training samples as  $\{(\boldsymbol{\xi}_{i1}, \dots, \boldsymbol{\xi}_{ip}, Y_i)\}_{i=1}^n$ .

In the following, we assume that there exists a class of discriminant functions  $\{f_k\}_{k=1}^K$  of  $\{\boldsymbol{\xi}_1, \dots, \boldsymbol{\xi}_p\}$ , such that the class label  $Y$  is assigned to class  $k'$  if  $k' = \arg \max_{k=1, \dots, K} f_k(\boldsymbol{\xi}_1, \dots, \boldsymbol{\xi}_p)$ . In the substantial literature concerning functional data classification, discriminant functions are traditionally typified as linear or quadratic, a methodology underscored by parametric strategies for estimating model coefficients [5, 6, 4, 19, 22]. While effective within their model constraints, these methods critically rely on specific distributional assumptions, making them vulnerable to underperformance when these assumptions are violated. Countering this limitation, recent innovations by [17] and [16] have shifted the paradigm, considering a convoluted structure in the discriminant function. This groundbreaking non-parametric approach accommodates the intricacies of functional data, employing DNNs to navigate the classification conundrum. The novelty of this strategy lies in its resilience against the unpredictable nature of functional data distributions, representing a substantial advancement over traditional methods constrained by rigid model specifications.

## 2.2. Deep neural network classifier

Before constructing the classifier, we first obtain the estimation of FPCs  $\{\boldsymbol{\xi}_j\}_{j=1}^p$  from  $\{\mathbf{X}_i\}_{i=1}^n$ . For  $j = 1, \dots, p$  and  $k \in \{1, \dots, K\}$ , define sample covariance function

$$\hat{\Omega}_{j|k}(\mathbf{s}_j, \mathbf{s}'_j) = \frac{1}{n_k} \sum_{i \in I_k} (X_{ij}(\mathbf{s}_j) - \bar{X}_{j|k}(\mathbf{s}_j))(X_{ij}(\mathbf{s}'_j) - \bar{X}_{j|k}(\mathbf{s}'_j)), \quad \mathbf{s}_j, \mathbf{s}'_j \in [0, 1]^{d_j},$$

where  $I_k$  is the collection of  $i$  such that  $Y_i = k$ ,  $n_k = |I_k|$  is the sample size,  $\bar{X}_{j|k}(\mathbf{s}_j) = n_k^{-1} \sum_{i \in I_k} X_{ij}(\mathbf{s}_j)$  is the sample mean function of class  $k$ . The spectral decomposition for  $\widehat{\Omega}_{j|k}(\mathbf{s}_j, \mathbf{s}'_j)$  is given by

$$\widehat{\Omega}_{j|k}(\mathbf{s}_j, \mathbf{s}'_j) = \sum_{\ell=1}^{\infty} \widehat{\lambda}_{j|k,\ell} \widehat{\phi}_{j|k,\ell}(\mathbf{s}_j) \widehat{\phi}_{j|k,\ell}(\mathbf{s}'_j), \mathbf{s}_j, \mathbf{s}'_j \in [0, 1]^{d_j}.$$

The sample data function  $X_{ij}(\mathbf{s}_j)$ , under  $Y_i = k$ , can be approximated as  $X_{ij}(\mathbf{s}_j) \approx \sum_{\ell=1}^{\infty} \widehat{\xi}_{ij,\ell} \widehat{\phi}_{j|k,\ell}(\mathbf{s}_j)$ , where  $\widehat{\xi}_{ij,\ell} = \langle X_{ij} - \bar{X}_{j|k}, \widehat{\phi}_{j|k,\ell} \rangle$ . Intuitively,  $\widehat{\boldsymbol{\xi}}_{ij} := (\widehat{\xi}_{ij,1}, \widehat{\xi}_{ij,2}, \dots)$  is an estimator of unobservable  $\boldsymbol{\xi}_{ij}$ , and it is natural to design classifiers based on  $\widehat{\boldsymbol{\xi}}_{ij}$ 's.

Given intrinsically infinite dimensional functional observations with potential large value  $p$ , we need a practical representation of  $\widehat{\boldsymbol{\xi}}_j$ . Define a truncation vector  $\mathbf{r} \in \mathbb{R}^p$  and  $\mathbf{r} = (r_j)_{j=1,\dots,p}^T$ , such that the truncated FPCs are denoted by  $\widehat{\boldsymbol{\xi}}_j^{(r_j)} = (\widehat{\xi}_{j,1}, \widehat{\xi}_{j,2}, \dots, \widehat{\xi}_{j,r_j})^T$ . Particularly, the selection of  $\mathbf{r}$  plays a crucial role in the classification performance, for which we employ a train-test validation approach to determine the optimal  $\mathbf{r}$  in Section 3.

Equipped with the  $\left\{ \widehat{\boldsymbol{\xi}}_j^{(r_j)} \right\}_{j=1}^p$ , we explore the class of residual feed-forward neural networks, denoted as  $\mathcal{D}$ . These networks are not only noted for the ease of training [7], but are also acclaimed for their versatility in serving as universal approximators for a diverse array of function classes [11]. Let  $\mathbf{W}$  be a collection of weight matrices  $W_l \in \mathbb{R}^{q_l \times q_{l+1}}$ . In the  $l$ -th ( $l = 1, \dots, L$ ) hidden layer of the neural network, there are  $q_{l+1}$  nodes and  $q_l$  nodes in the previous layer. The residual feed-forward neural networks is defined as

$$\mathcal{D} = \left\{ f_{\mathbf{b}, \mathbf{W}} : f = \sigma^* \left( \sum_{j=1}^p \mathbf{b}_j^T \widehat{\boldsymbol{\xi}}_j^{(r_j)} + g_{\mathbf{W}} \left( \widehat{\boldsymbol{\xi}}_1^{(r_1)}, \dots, \widehat{\boldsymbol{\xi}}_p^{(r_p)} \right) \right) \right\}, \quad (2.2)$$

where  $\mathbf{b} = (\mathbf{b}_1^T, \dots, \mathbf{b}_p^T)^T$  denotes the weights for residual layer and  $\sigma^*$  is an activation function to be selected according to the class number. Additionally, note that  $q_1 = \sum_{j=1}^p r_j$ , which is the number of inputs  $\left\{ \widehat{\boldsymbol{\xi}}_j^{(r_j)} \right\}_{j=1}^p$ . Any generic nonlinear function  $g$  has the composition representation [14, 16]

$$g(\mathbf{x}) = W_L \sigma W_{L-1} \sigma \dots W_2 \sigma W_1 \mathbf{x}, \quad \mathbf{x} \in \mathbb{R}^{q_1}, \quad (2.3)$$

where  $\sigma$  is the activation function, such as ReLU. We estimate the classifier  $f$  by optimizing the following problem:

$$\widehat{f} = \arg \min_{f \in \mathcal{D}} n^{-1} \sum_{i=1}^n \mathcal{L} \left( Y_i, f \left( \widehat{\boldsymbol{\xi}}_{i1}^{(r_1)}, \dots, \widehat{\boldsymbol{\xi}}_{ip}^{(r_p)} \right) \right), \quad (2.4)$$

where the loss function  $\mathcal{L}$  is chosen regarding the classification task.

For the binary classification with  $K = 2$ , one common option for  $\mathcal{L}$  is the hinge loss. Consequently, adjusted by the label  $Y_i = \{1, 2\}$ , the loss function  $\mathcal{L}$  is defined as  $\mathcal{L}(Y_i, f(\cdot)) = \max(1 - (2Y_i - 3)f(\cdot), 0)$ . The optimizer of Equation (2.4) is essentially the estimate of log-likelihood ratio of the two classes  $f^*$ , thus

the activation function  $\sigma^*$  is the identity function, and the new label will be estimated by the sign of  $\hat{f}$ , i.e.,

$$\hat{Y} = \begin{cases} 2, & \hat{f}(\hat{\boldsymbol{\xi}}_1^{(r_1)}, \dots, \hat{\boldsymbol{\xi}}_p^{(r_p)}) \geq 0, \\ 1, & \hat{f}(\hat{\boldsymbol{\xi}}_1^{(r_1)}, \dots, \hat{\boldsymbol{\xi}}_p^{(r_p)}) < 0. \end{cases} \quad (2.5)$$

In general, for the multi-class classification with  $K \geq 2$ , the activation function  $\sigma^*$  is selected as the  $K$ -dimensional softmax function  $\sigma^*(\mathbf{z}) = \left( \frac{\exp(z_1)}{\sum_{k=1}^K \exp(z_k)}, \dots, \frac{\exp(z_K)}{\sum_{k=1}^K \exp(z_k)} \right)$  for  $\mathbf{z} = (z_1, \dots, z_K) \in \mathbb{R}^K$ . Define the label as  $\mathbf{y} = (y_1, \dots, y_K)^\top$ , such that  $y_k = 1$  if  $Y = k$  and 0 otherwise. The loss function  $\mathcal{L}$  is the cross-entropy function

$$\mathcal{L}(Y_i, f(\hat{\boldsymbol{\xi}}_{i1}^{(r_1)}, \dots, \hat{\boldsymbol{\xi}}_{ip}^{(r_p)})) = -\mathbf{y}_i \log \left( f(\hat{\boldsymbol{\xi}}_{i1}^{(r_1)}, \dots, \hat{\boldsymbol{\xi}}_{ip}^{(r_p)}) \right), \quad (2.6)$$

where  $f(\hat{\boldsymbol{\xi}}_{i1}^{(r_1)}, \dots, \hat{\boldsymbol{\xi}}_{ip}^{(r_p)}) = (f_1(\hat{\boldsymbol{\xi}}_{i1}^{(r_1)}, \dots, \hat{\boldsymbol{\xi}}_{ip}^{(r_p)}), \dots, f_K(\hat{\boldsymbol{\xi}}_{i1}^{(r_1)}, \dots, \hat{\boldsymbol{\xi}}_{ip}^{(r_p)}))^\top$ . Cross-entropy loss is a frequently employed loss function. This metric measure the difference between the projected probability distribution and the actual probability distribution of the target classes. The cross-entropy loss will be substantial, for instance, if the model forecasts a low probability for the right class but a high probability for the incorrect class. The optimizer  $\hat{f}_k$  is the estimation of conditional probability density  $f_k$  under the  $k$ -th class, which is between 0 and 1 confined by the softmax function. Therefore, the new label is assigned by  $\hat{Y} = \arg \max_{\{k=1, \dots, K\}} \left\{ k : \hat{f}_k(\hat{\boldsymbol{\xi}}_{i1}^{(r_1)}, \dots, \hat{\boldsymbol{\xi}}_{ip}^{(r_p)}) \right\}$ .

The following theorem presents the uniform approximation theory of our proposed neural network class to the Bayesian classifier. For the sake of space limit, the function classes  $\mathcal{G}$  and  $\{\mathcal{G}_k\}_{k=1}^K$  and related notations  $\alpha_1$  and  $\alpha_2$  are introduced in the Appendix. We denote  $s$  as the number of non-zero weights for the sparse neural network class  $\mathcal{D}$ .

**Assumption 1.** Given any  $\epsilon > 0$  and  $r_j \in \mathbb{N}^+$ ,  $j = 1, \dots, p$ , the network class  $\mathcal{D}$  satisfies

$$L \asymp \log_2(\epsilon^{-1}), \quad \|\mathbf{q}\|_\infty \asymp \max \left\{ \sum_{j=1}^p r_j, \epsilon^{-\alpha_1} \right\}, \quad s \asymp \log_2(1/\epsilon) (\epsilon^{-\alpha_1}), \quad \|\mathbf{W}\|_\infty \asymp \epsilon^{-1},$$

where  $\alpha_1$  is a constant depending on  $\mathcal{G}$ .

**Assumption 2.** Given any  $\epsilon > 0$  and  $r_j \in \mathbb{N}^+$ ,  $j = 1, \dots, p$ , the network class  $\mathcal{D}$  satisfies  $L \asymp \log_2(\epsilon^{-1})$ ,  $\|\mathbf{q}\|_\infty \asymp \max \left\{ \sum_{j=1}^p r_j, \epsilon^{-\alpha_2} \right\}$ ,  $s \asymp \log_2(1/\epsilon) (\epsilon^{-\alpha_2})$ , where  $\alpha_2$  is a constant depending on  $\{\mathcal{G}_k\}_{k=1}^K$ .

To better illustrate the following theorem for binary classification ( $K = 2$ ), for any  $\epsilon > 0$ , we define the set  $\mathcal{B}(\epsilon) = \{\mathbf{x} \in \mathbb{R}^{q_1} : |\mathbb{P}(Y = 1 | \boldsymbol{\xi}^{(r)} = \mathbf{x}) - 1/2| > 2\epsilon\}$ , where  $\boldsymbol{\xi}^{(r)} = \left( (\boldsymbol{\xi}_1^{(r_1)})^\top, \dots, (\boldsymbol{\xi}_p^{(r_p)})^\top \right)^\top$ . Without loss of generality, we assume that  $\mathbb{P}(Y = 1 | \boldsymbol{\xi}^{(r)} = \mathbf{x}) \neq 1/2, \forall \mathbf{x} \in \mathbb{R}^{q_1}$ . Note that this set controls the distance between the regression function and 1/2, and its size is decreasing with  $\epsilon$ . When  $\epsilon \rightarrow 0$ ,  $\mathcal{B} \rightarrow \mathbb{R}^{q_1}$ , reflecting the fact that  $\mathcal{B}$  expands to cover the entire space.

**Theorem 2.1.** *Given any universal  $\epsilon > 0$ , when the activation function  $\sigma$  in (2.3) is ReLU, it follows that: (a) For  $K = 2$  and identity function  $\sigma^*$  in (2.2), if  $f_1, f_2 \in \mathcal{G}$ , there exists  $\widehat{f} \in \mathcal{D}$  satisfying Assumption 1, such that  $\widehat{f}(\mathbf{x}) = f^*(\mathbf{x})$ ,  $\mathbf{x} \in \mathcal{B}(\epsilon)$ , where  $f^*$  is the Bayesian decision function of truncated scores; (b) For  $K \geq 2$  and softmax function  $\sigma^*$  in (2.2), if  $f_k \in \mathcal{G}_k$  and  $\min_{k=1, \dots, K} \|f_k\|_\infty \geq \epsilon > 0$ , there exist  $\widehat{f}_k \in \mathcal{D}$  satisfying Assumption 2, such that  $\|\widehat{f}_k - f_k\|_\infty \leq \epsilon$ ,  $k = 1, \dots, K$ .*

Theorem 2.1 demonstrates the universal approximation theory using ReLU activation function for both binary and multi-class classification scenarios. As discussed in Section 2.2,  $f^*$  is essentially the log ratio of probabilities of two classes, and Theorem 2.1 (a) indicates that in any subset of  $\mathbb{R}^{q_1}$ , with a well selected DNN structure, we are able to construct the Bayesian decision rule exactly. For multi-class classification with the softmax function, it is crucial to accurately approximate the conditional probability  $f_k$ , and Theorem 2.1 (b) shows that any  $f_k$  can be well approximated with a finely tuned architecture. We provide the proof in a separate file upon request.

### 2.3. Functional feature selection

Effective variable selection can identify functional covariates that provide significant predictive power. In the following, we consider a regularization approach with constraints on weights. This architecture involves multiple layers of neurons with Lasso regularization applied to the weights connecting the neurons in each layer. During training, the Lasso penalty term is added to the loss function, promoting a sparse solution by shrinking some weights towards zero. This encourages the model to focus on the most informative features while discarding irrelevant ones. Specifically, we estimate  $f(\cdot)$  by minimizing

$$\arg \min_{\widehat{f} \in \mathcal{D}} n^{-1} \sum_{i=1}^n \mathcal{L} \left( Y_i, \widehat{f} \left( \widehat{\boldsymbol{\xi}}_{i1}^{(r_1)}, \dots, \widehat{\boldsymbol{\xi}}_{ip}^{(r_p)} \right) \right) + \lambda \sum_{j=1}^p P_j(\mathbf{b}_j), \text{ s.t. } \|W_1^{(j)}\|_\infty \leq C \|\mathbf{b}_j\|, \quad j = 1, \dots, p, \quad (2.7)$$

where  $P_j(\cdot) : \mathbb{R}^{r_j} \rightarrow \mathbb{R}$  is the penalty function for regularization; the hierarchy coefficient  $C$  controls the relative strength of the linear and nonlinear components; the  $L_1$  penalty coefficient  $\lambda$  controls the complexity of the fitted model; and  $W_1^{(j)}$  is the sub-matrix of  $W_1$  connected to  $\widehat{\boldsymbol{\xi}}_{ij}^{(r_j)}$ . The regularizers  $P_j(\cdot)$  impose sparsity at the group level for entire  $\mathbf{b}_j$ , meaning that the entire groups of FPCs can be shrunk to zero. The estimated  $\{\mathbf{b}_j\}_{j=1}^p$  automatically estimates the true sparse set  $\mathcal{A} = \{j : \|\mathbf{b}_j\| \neq 0, j \in \{1, \dots, p\}\}$ . The constraints are designed to calibrate the level of non-linearity attributed to feature  $j$ . If the entire vector  $\mathbf{b}_j$  are forced to be zero, then all weights connected to the neural network that are related to  $\widehat{\boldsymbol{\xi}}_{ij}^{(r_j)}$  are effectively shrunk to be zero, leading to the exclusion of the  $j$ th feature from the model. This idea extends the LassoNet algorithms proposed in [9] for i.i.d. high-dimensional data, where  $P_j$  are set to be the group-LASSO



penalty. The crucial distinction lies in the inclusion of the truncation vector  $\mathbf{r}$ , which greatly influences both classification accuracy and feature selection efficiency.

The selection of the tuning parameters is important in practice. Cross-validation is a popular approach and is integrated into LassoNet, making it an intuitive first choice when extending the LassoNet algorithm. We name the associated algorithm “f-DNN”. See f-DNN algorithm in Section 4 for details. However, we have observed that its performance for selecting functional features is not satisfactory. [15] recently proposed high-dimensional BIC for ultra-high dimensional regression when  $p$  is much larger than  $n$ . Let  $\boldsymbol{\eta} = (\mathbf{r}, L, \mathbf{q}, \gamma, \lambda)$  be the tuning parameter set for loss function  $\mathcal{L}$ , where  $\gamma$  is the dropout rate of neurons. Note that any fixed  $(\mathbf{r}, L, \mathbf{q}, u)$  determines the architecture of the neural network class  $\mathcal{D}$ . Motivated by [15], we choose tuning parameters  $\boldsymbol{\eta}$  that minimizes the following functional data BIC criterion (F-BIC) for fB-DNN classification:

$$\text{F-BIC}(\boldsymbol{\eta}) = \sum_{i \in \mathcal{I}_2} \sum_{k=1}^K \mathbb{I}(Y_i = k) \left\{ -\log \widehat{f}_{ik} \left( \widehat{\boldsymbol{\xi}}_{i1}^{(r_1)}, \dots, \widehat{\boldsymbol{\xi}}_{ip}^{(r_p)}; \boldsymbol{\eta} \right) \right\} + C_\tau p_0(\boldsymbol{\eta}) \frac{\log p}{n}, \quad (2.8)$$

where the constant  $C_\tau = 3 \times 10^\tau$ . In practice, we recommend  $\tau = -1, 0, 1, 2$ . We name the associated algorithm “fB-DNN”. The following Algorithms 1 and 2 describe the fB-DNN procedure, and Proposition 2.1 validates the algorithms. The proof of Proposition 2.1 is provided in a separate file upon request.

**Proposition 2.1.** *If  $0 \leq r_j < \infty$ ,  $j = 1, \dots, p$ , the solution to Algorithm 2 is the global optimum of the constraint objective function (2.7).*

Under Proposition 2.1, when the DNN architecture is properly selected, the following theorem provides convergence rates of our proposed classifier to the Bayes classifier. Denote the true conditional density function of  $(\boldsymbol{\xi}_1, \dots, \boldsymbol{\xi}_p)$  as  $\{f_{0k}\}_{k=1}^K$ . The orders  $\alpha_1^*$  and  $\alpha_2^*$  are defined in (7.1) in Appendix.

**Theorem 2.2.** *When the activation function  $\sigma$  in (2.3) is ReLU, it follows that: (a) For  $K = 2$  and identity function  $\sigma^*$  in (2.2), under Assumption 3 in the Appendix, if  $f_1, f_2 \in \mathcal{G}$  and the hinge loss is employed,  $\widehat{Y}$  defined in (2.5) satisfies*

$$\mathbb{P}(\widehat{Y} \neq Y) - \mathbb{P}(\widehat{Y}^* \neq Y) \lesssim n^{-\alpha_1^*} \log^3 n,$$

where  $\widehat{Y}^*$  is the class derived by the Bayes classifier of  $(\boldsymbol{\xi}_1, \dots, \boldsymbol{\xi}_p)$ ; (b) For  $K \geq 2$  and softmax function  $\sigma^*$  in (2.2), under Assumption 4 in the Appendix, if  $f_k \in \mathcal{G}_k$  and cross-entropy loss function (2.6) is employed, the optimizer  $\widehat{f}$  in (2.7) satisfies

$$\mathbb{E} \left[ \sum_{k=1}^K f_{0k}(\boldsymbol{\xi}_1, \dots, \boldsymbol{\xi}_p) \left( c_0 \wedge \log \left( \frac{f_{0k}(\boldsymbol{\xi}_1, \dots, \boldsymbol{\xi}_p)}{\widehat{f}_k(\boldsymbol{\xi}_1^{(r_1)}, \dots, \boldsymbol{\xi}_p^{(r_p)})} \right) \right) \right] \lesssim n^{-\alpha_2^*} \log^3 n,$$

where  $c_0$  is a relatively large constant.

**Algorithm 1** fB-DNN algorithm for functional data classification and feature selection1: **Inputs:**

Functional data  $\{\mathbf{X}_i\}_{i=1}^n$ , class label  $\{Y_i\}_{i=1}^n$ , basis functions  $\{\widehat{\phi}_{j|k,1}, \widehat{\phi}_{j|k,2}, \dots\}_{j=1}^p$ ,  
epoch number  $B$ , hierarchy coefficient  $C$ , learning rate  $\alpha$ , training index  $\mathcal{I}_1$ , validation index  $\mathcal{I}_2$ ,  
tuning candidates:  $\{\boldsymbol{\eta}_1, \dots, \boldsymbol{\eta}_M\}$  with initial value  $\lambda_0$  and path multiplier  $\delta$ ,

2: **for**  $\ell = 1, \dots, M$  **do**3: Apply Algorithm 2 on  $\{\mathbf{X}_i, Y_i\}_{i \in \mathcal{I}_1}$  and obtain  $p_0(\boldsymbol{\eta}_\ell)$ ,  $\mathbf{b}(\boldsymbol{\eta}_\ell)$  and  $\mathbf{W}(\boldsymbol{\eta}_\ell)$ 4: Obtain the estimated probability  $\widehat{f}_{ik}(\widehat{\boldsymbol{\xi}}_{i1}^{(r_1)}, \dots, \widehat{\boldsymbol{\xi}}_{ip}^{(r_p)}; \boldsymbol{\eta}_\ell)$ ,  $i \in \mathcal{I}_2$ ,  $k = 1, \dots, K$ , by5: **end for**6: Calculate the F-BIC for the validation dataset. Obtain  $\boldsymbol{\eta}^* = \arg \min_{\boldsymbol{\eta} \in \{\boldsymbol{\eta}_1, \dots, \boldsymbol{\eta}_M\}} \text{F-BIC}(\boldsymbol{\eta})$ 7: Obtain the weights  $\widehat{\mathbf{b}} \equiv \mathbf{b}(\boldsymbol{\eta}^*)$  and  $\widehat{\mathbf{W}} \equiv \mathbf{W}(\boldsymbol{\eta}^*)$ , and the selected index set  $\widehat{\mathcal{A}} = \{j : \|\widehat{\mathbf{b}}_j\| \neq 0\}$ 8: **Outputs:**  $\widehat{\mathbf{b}}$ ,  $\widehat{\mathbf{W}}$  and  $\widehat{\mathcal{A}}$ **Algorithm 2** Training penalty term in Model (2.7)1: **Inputs:**

Functional data  $\{\mathbf{X}_i\}_{i=1}^n$ , class label  $\{Y_i\}_{i=1}^n$ , truncation vectors  $\mathbf{r}$ , basis functions  
 $\{\widehat{\phi}_{j|k,1}, \dots, \widehat{\phi}_{j|k,r_j}\}_{j=1}^p$ , number of hidden layer  $L$ , number of neurons  $\mathbf{q}$ , dropout rate  $\gamma$ , epoch  
number  $B$ , hierarchy coefficient  $C$ , path multiplier  $\delta$ , learning rate  $\alpha$ , initial tuning parameter  $\lambda_0$ .

2: Initialize  $\lambda = \lambda_0$ ,  $p_0 = p$ 3: Obtain  $\xi_{ij,\ell} = \langle X_{ij}, \widehat{\phi}_{j|k,\ell} \rangle$ ,  $i = 1, \dots, n$ ,  $j = 1, \dots, p$ ,  $\ell = 1, \dots, r_j$ 4: **while**  $p_0 \geq 1$  **do**  $\lambda \leftarrow (1 + \delta)\lambda$ 5: **for**  $b = 1, 2, \dots, B$  **do**6: Compute  $\nabla_{\mathbf{b}} \mathcal{L}$ ,  $\nabla_{\mathbf{W}} \mathcal{L}$  by backpropagation7: Update  $\mathbf{b} \leftarrow \mathbf{b} - \alpha \nabla_{\mathbf{b}} \mathcal{L}$ ,  $\mathbf{W} \leftarrow \mathbf{W} - \alpha \nabla_{\mathbf{W}} \mathcal{L}$ 8: **for**  $j = 1, \dots, p$  **do**9: Update  $\mathbf{b}_j$  and  $W_1^{(j)}$  via Algorithm 3 in Appendix10: **end for**11: **end for**12: Update  $p_0$  to be the number of non-zero coordinates of  $\|\mathbf{b}_j\|$ 13: **end while**14: **Outputs:**  $p_0$  and  $\mathbf{b}$ 

### 3. Implementation

Our proposed neural networks are implemented using Python within the PyTorch framework. Specifically, the feedforward neural network is constructed based upon the number of hidden layer  $L$ , number of neurons in each hidden layer  $q_l$ ,  $l = 1, \dots, L$ , and the dropout rate  $\gamma$ . Throughout, the epoch number and batch size for training the neural network are fixed before the training process. Practically, we choose the epoch number to be moderately large, as long as the results are stable, and the batch size equals  $2^{\lfloor \log n \rfloor}$ , where  $\lfloor \cdot \rfloor$  denotes the floor function. We conduct Algorithm 1 to choose the best neural network structure and the optimal truncation of FPCs. For all numerical studies, we apply Algorithm 1 by randomly assigning 60% data to the training set and 20% data to the validation set, and the remaining 20% data are used as a testing set to obtain the classification accuracy. To optimize the training process with respect to objective (2.7), we use Adam optimizer with a learning rate of  $\alpha = 0.001$  to train the initial model. The path multiplier is stable across all simulation settings, where we let  $\delta = 0.02$ . We choose hierarchy coefficient  $C = 10$  as default. The optimization of Algorithm 2 with respect to the tuning parameter  $\lambda$  adopts the

dense-to-sparse warm start approach. This approach yields effective performance with strong generalization ability [9]. Python codes and examples for the proposed fB-DNN algorithms are available on GitHub (<https://github.com/ShuoyangWang/fB-DNN>).

#### 4. Simulation studies

In this section, we assess the effectiveness of our proposed method for handling 2D functional data and a mixture of 1D and 2D functional data. To gauge the comparative performance, we consider four alternative methods, f-SVM, f- $k$ NN, f-DNN and mfDNN [16]. Support vector machine (SVM) and  $k$ -nearest neighbor ( $k$ NN) are efficient classifiers designed for high-dimensional i.i.d. observations. To make these methods directly applicable to functional data, we adapt them by utilizing the inputs as FPCs extracted from all functional features. The realization is via the R packages `e1071` and `class`, respectively, where the tuning parameter candidates for the penalty term are generated by default. For f-SVM, we choose linear kernel and polynomial kernel with degree 3. For f- $k$ NN,  $k$  is selected by cross-validation. With f-DNN, we can demonstrate the comparative performance in selection and classification performance of our proposed F-BIC. Note that the f-DNN procedure follows Algorithm 1, with a modification that substitutes the F-BIC criterion with the minimization of misclassification risk using 5-fold cross-validation. Specifically, in Algorithm 1, Step 6 is substituted with  $\boldsymbol{\eta}^* = \arg \min_{\boldsymbol{\eta} \in \{\boldsymbol{\eta}_1, \dots, \boldsymbol{\eta}_M\}} \text{MR}(\boldsymbol{\eta})$ , where  $\text{MR}(\boldsymbol{\eta}) = |\mathcal{I}_2|^{-1} \sum_{i \in \mathcal{I}_2} \mathbb{I}(Y_i \neq \widehat{Y}_i(\boldsymbol{\eta}))$  is the empirical misclassification risk. To our knowledge, the mfDNN algorithm proposed by [16] stands as the only publicly available algorithm tailored for both 1D and 2D functional data. Except for fB-DNN and f-DNN, the rest of competitors are not equipped with a regularization term to conduct feature selection. Performance of selection is compared only between f-DNN and fB-DNN. Results are based on 50 simulations.

##### 4.1. 2D functional data case

We generated functional data  $X_{ij}(s, t) = \sum_{\ell=1}^5 \xi_{ij,\ell} \phi_\ell(s, t) + \epsilon_{ij}(s, t)$ ,  $i = 1, \dots, n_k$ ,  $k = 1, 2, 3$ ,  $s, t \in [0, 1]$ , where  $\phi_1(s, t) = s$ ,  $\phi_2(s, t) = t$ ,  $\phi_3(s, t) = st$ ,  $\phi_4(s, t) = s^2$ ,  $\phi_5(s, t) = t^2$ . The true feature set to distinguish the three classes is  $\mathcal{A} = \{1, 2, 3, 4, 5\}$ . We generated the features in  $\mathcal{A}^c = \{6, 7, \dots, p\}$  by letting  $\boldsymbol{\xi}_{ij}|Y_i = k \sim \mathcal{N}((0, 0, 0, 0, 0)^\top, \text{diag}(1, 0.64, 0.36, 0.16, 0.04))$ ,  $j = 6, 7, \dots, p$ , where  $\boldsymbol{\xi}_{ij} = (\xi_{ij,1}, \xi_{ij,2}, \xi_{ij,3})^\top$ . The features in  $\mathcal{A}$  were generated by the following three settings:

**Model I (Gaussian data with high separability):** For  $j = 1, \dots, 5$ , let

$$(\boldsymbol{\xi}_{ij}|Y_i = 1) \sim \mathcal{N}((2.5, 2, 1.5, 1, 0.5)^\top, \text{diag}(25, 16, 9, 4, 1));$$

$$(\boldsymbol{\xi}_{ij}|Y_i = 2) \sim \mathcal{N}((-2.5, -2, -1.5, -1, -0.5)^\top, \text{diag}(9, 4, 2.25, 1, 0.25));$$

$$\text{and } (\boldsymbol{\xi}_{ij}|Y_i = 3) \sim \mathcal{N}((0, 0, 0, 0, 0)^\top, \text{diag}(1, 0.64, 0.36, 0.16, 0.04)).$$

**Model II (Gaussian data with low separability):** For  $j = 1, \dots, 5$ , let

$$(\xi_{ij}|Y_i = 1) \sim \mathcal{N}((0.5, 0.5, 0.5, 0.5, 0.5)^\top, \text{diag}(25, 16, 9, 4, 1));$$

$$(\xi_{ij}|Y_i = 2) \sim \mathcal{N}((-0.5, -0.5, -0.5, -0.5, -0.5)^\top \text{diag}(9, 4, 2.25, 1, 0.25));$$

$$\text{and } (\xi_{ij}|Y_i = 3) \sim \mathcal{N}((0, 0, 0, 0, 0)^\top, \text{diag}(1, 0.64, 0.36, 0.16, 0.04)).$$

**Model III (Non-Gaussian data):** For  $j, \ell = 1, \dots, 5$ , let

$$(\xi_{i,j,\ell}|Y_i = 1) \sim \text{Exp}(\theta_\ell), \text{ where } \theta_1 = 0.1, \theta_2 = 0.12, \theta_3 = 0.14, \theta_4 = 0.16, \theta_5 = 0.18;$$

$$(\xi_{i,j,\ell}|Y_i = 2) \sim t_{2\ell+1}(3); (\xi_{ij}|Y_i = 3) \sim \mathcal{N}((0, 0, 0, 0, 0)^\top, \text{diag}(1, 0.64, 0.36, 0.16, 0.04)).$$

To mimic our real data of 2D PET scans, we consider functional features  $p = 50, 100$ , with sample size for each group  $n_k \in \{100, 200\}$ ,  $k = 1, 2, 3$ . Additionally, we chose  $s$  and  $t$  on  $m$  evenly spaced grid points on  $[0, 1]$ , with  $m = 30$  and  $m = 60$  to represent relatively sparse and dense grid points. For each model, we observe the functional data on  $30 \times 30$  or  $60 \times 60$  grid points over  $[0, 1]^2$ . The chosen optimal numbers of FPCs, hidden layers and neurons in each layer vary by different replicates. The candidates for the number of FPCs are  $\{3, 5, 10, 15, 20, 25\}$ ; for the number of hidden layers  $\{1, 2, 3\}$ ; and for the number of neurons in each layer  $\{100, 300\}$ . Table 1 and 2 present the exact match rate (EMR) which is defined as the proportion that the selected functional features exactly match the true functional features, and the average number of falsely selected features (FP). These two quantities describe the ability of various classifiers for feature selection. To measure the classification accuracy, we report the average true classification rates.

Several noteworthy findings emerge from the analysis of the two tables. Firstly, in Table 1, both fB-DNN and f-DNN demonstrate superior performance in Models I and III compared to Model II. This discrepancy is expected given the low separability between classes in Model II, which makes classification inherently more challenging. Secondly, fB-DNN exhibits an improved EMR with increasing sample sizes, unlike f-DNN, where larger sample sizes lead to significantly worse performance in Model II. This observation suggests that f-DNN struggles to efficiently eliminate redundant information. This finding is unanimously supported by the notably high FP observed in f-DNN across all three models. Lastly, in Table 2, fB-DNN and f-DNN display comparable classification accuracy and both exhibit an enhanced accuracy with increasing sample sizes. On the other hand, mfDNN and f-SVM alternative classifiers consistently lag behind, particularly in scenarios with a higher number of redundant features. f- $k$ NN classifier has comparable classification rates in Models I and III. However, f- $k$ NN has much lower classification accuracy in Model II. In summary, the simulation results underscore the superiority of the proposed fB-DNN method over alternative deep learning approaches when classifying 2D functional data.

TABLE 1

Performance of feature selection for Models I, II, and III by the exact match rate, EMR (average number of incorrectly selected false features, FP).

Model	Method	$n_k$	$m = 30$		$m = 60$	
			$p = 50$	$p = 100$	$p = 50$	$p = 100$
I	fB-DNN	100	<b>0.90(0.12)</b>	<b>0.90(0.06)</b>	<b>0.90(0.06)</b>	<b>0.90(0.30)</b>
		200	<b>0.92(1.20)</b>	<b>0.92(0.12)</b>	<b>0.92(0.10)</b>	<b>0.92(0.06)</b>
	f-DNN	100	0.64(4.68)	0.40(14.96)	0.58(7.48)	0.54(10.50)
		200	0.26(14.08)	0.20(24.30)	0.22(10.44)	0.18(28.18)
II	fB-DNN	100	<b>0.60(0.72)</b>	<b>0.46(0.94)</b>	<b>0.72(0.50)</b>	<b>0.70(0.56)</b>
		200	<b>0.68(2.16)</b>	<b>0.54(2.02)</b>	<b>0.76(1.10)</b>	<b>0.74(0.76)</b>
	f-DNN	100	0.26(11.42)	0.06(22.82)	0.18(13.76)	0.24(18.66)
		200	0.08(31.66)	0.10(57.30)	0.08(28.10)	0.06(50.28)
III	fB-DNN	100	<b>0.98(0.04)</b>	<b>0.96(0.04)</b>	<b>0.98(0.04)</b>	<b>0.96(0.12)</b>
		200	<b>1.00(0.00)</b>	<b>1.00(0.00)</b>	<b>1.00(0.00)</b>	<b>1.00(0.00)</b>
	f-DNN	100	0.84(3.44)	0.80(1.38)	0.76(3.06)	0.84(0.92)
		200	0.90(2.46)	0.98(2.72)	0.88(2.26)	0.96(2.86)

TABLE 2

The average true classification rates for Models I, II, and III.

Model	Method	$n_k$	$m = 30$		$m = 60$	
			$p = 50$	$p = 100$	$p = 50$	$p = 100$
I	fB-DNN	100	<b>0.974</b>	<b>0.964</b>	<b>0.970</b>	0.969
		200	0.980	<b>0.982</b>	0.981	<b>0.983</b>
	f-DNN	100	0.964	0.964	0.968	<b>0.970</b>
		200	<b>0.982</b>	0.980	<b>0.983</b>	0.981
	mfDNN	100	0.935	0.296	0.936	0.298
		200	0.957	0.303	0.954	0.304
	f-SVM	100	0.896	0.817	0.895	0.821
		200	0.928	0.894	0.928	0.897
	f-kNN	100	0.909	0.906	0.909	0.906
		200	0.933	0.931	0.933	0.931
II	fB-DNN	100	<b>0.854</b>	<b>0.850</b>	0.846	<b>0.857</b>
		200	<b>0.872</b>	<b>0.871</b>	<b>0.869</b>	<b>0.871</b>
	f-DNN	100	0.854	0.845	<b>0.850</b>	0.850
		200	0.866	0.869	0.864	0.866
	mfDNN	100	0.677	0.292	0.669	0.300
		200	0.751	0.301	0.751	0.306
	f-SVM	100	0.579	0.508	0.586	0.511
		200	0.647	0.556	0.654	0.564
	f-kNN	100	0.588	0.593	0.587	0.594
		200	0.667	0.643	0.667	0.643
III	fB-DNN	100	<b>0.964</b>	<b>0.961</b>	<b>0.964</b>	0.957
		200	<b>0.966</b>	<b>0.968</b>	<b>0.978</b>	<b>0.961</b>
	f-DNN	100	0.945	0.952	0.953	<b>0.959</b>
		200	0.959	0.961	0.961	0.955
	mfDNN	100	0.872	0.302	0.876	0.297
		200	0.934	0.312	0.931	0.315
	f-SVM	100	0.933	0.867	0.930	0.865
		200	0.959	0.939	0.957	0.937
	f-kNN	100	0.920	0.923	0.921	0.923
		200	0.932	0.934	0.932	0.934

TABLE 3  
Performance of feature selection for Models IV, V, and VI by the exact match rate, EMR (average number of incorrectly selected false features, FP).

Model	Method	$n_k$	$m = 30$		$m = 60$	
			$p = 80$	$p = 130$	$p = 80$	$p = 130$
IV	fB-DNN	100	<b>0.88(0.14)</b>	<b>0.74(0.32)</b>	<b>0.88(0.10)</b>	<b>0.82(0.28)</b>
		200	<b>0.86(0.28)</b>	<b>0.86(0.38)</b>	<b>0.86(0.18)</b>	<b>0.84(0.34)</b>
	f-DNN	100	0.26(10.04)	0.14(16.52)	0.30(7.38)	0.20(18.06)
		200	0.06(36.96)	0.04(64.58)	0.04(38.00)	0.02(57.32)
V	fB-DNN	100	<b>0.84(0.08)</b>	<b>0.86(0.06)</b>	<b>0.86(0.02)</b>	<b>0.80(0.06)</b>
		200	<b>0.84(0.06)</b>	<b>0.84(0.06)</b>	<b>0.86(0.00)</b>	<b>0.84(0.04)</b>
	f-DNN	100	0.70(7.98)	0.62(14.52)	0.68(7.04)	0.58(16.96)
		200	0.28(14.98)	0.30(24.58)	0.32(12.72)	0.26(19.08)
VI	fB-DNN	100	<b>0.66(0.16)</b>	<b>0.60(0.36)</b>	<b>0.62(0.38)</b>	<b>0.62(0.66)</b>
		200	<b>0.82(0.20)</b>	<b>0.80(0.48)</b>	<b>0.84(0.10)</b>	<b>0.88(0.00)</b>
	f-DNN	100	0.56(1.26)	0.46(3.42)	0.40(2.90)	0.48(3.50)
		200	0.76(7.98)	0.52(2.10)	0.80(6.54)	0.80(3.18)

#### 4.2. Mixture of 1D and 2D functional data case

We first generated 1D functional data  $X_{ij}(s) = \sum_{\ell=1}^3 \xi_{ij,\ell} \phi_\ell(s) + \epsilon_{ij}(s)$ ,  $i = 1, \dots, n_k$ ,  $k = 1, 2, 3$ ,  $s \in [0, 1]$ , where  $\phi_1(s) = \log(s+2)$ ,  $\phi_2(s) = s$ ,  $\phi_3(s) = s^3$ . Across all settings, we consider 30 features of 1D data to mimic our real dataset, where we let the true feature be  $\mathcal{A}_1 = \{1, 2, 3\}$ . We generated the features in  $\mathcal{A}_1^c = \{4, 5, \dots, 30\}$  by letting  $\xi_{ij}|Y_i = k \sim \mathcal{N}((0, 0, 0)^\top, \text{diag}(1, 0.64, 0.36))$ ,  $j = 4, 5, \dots, 30$ , where  $\xi_{ij} = (\xi_{ij,1}, \xi_{ij,2}, \xi_{ij,3})^\top$ . For 2D functional data, we kept the same true feature set  $\mathcal{A}_2 = \{1, \dots, 5\}$  whose specifications followed the same details in Section 4.1. The features in  $\mathcal{A}_1$  and  $\mathcal{A}_2$  were generated by the following three settings:

**Model IV (Gaussian data with high separability)** For 1D functional data with  $j = 1, 2, 3$ , let

$$(\xi_{ij}|Y_i = 1) \sim \mathcal{N}((2.5, 2, 1.5)^\top, \text{diag}(25, 16, 9));$$

$$(\xi_{ij}|Y_i = 2) \sim \mathcal{N}((-2.5, -2, -1.5)^\top, \text{diag}(9, 4, 2.25));$$

$$(\xi_{ij}|Y_i = 3) \sim \mathcal{N}((0, 0, 0)^\top, \text{diag}(1, 0.64, 0.36)).$$
 2D functional data are generated as Model I.

**Model V (Gaussian data with low separability):** For 1D functional data with  $j = 1, 2, 3$ , let

$$(\xi_{ij}|Y_i = 1) \sim \mathcal{N}((0.5, 0.5, 0.5)^\top, \text{diag}(25, 16, 9));$$

$$(\xi_{ij}|Y_i = 2) \sim \mathcal{N}((-0.5, -0.5, -0.5)^\top, \text{diag}(9, 4, 2.25));$$

$$(\xi_{ij}|Y_i = 3) \sim \mathcal{N}((0, 0, 0)^\top, \text{diag}(1, 0.64, 0.36)).$$
 2D functional data are generated as Model II.

**Model VI (Non-Gaussian data):** For 1D functional data with  $j = 1, 2, 3$ , let

$$(\xi_{ij,\ell}|Y_i = 1) \sim \text{Exp}(\theta_\ell), \text{ where } \theta_1 = 0.1, \theta_2 = 0.15, \theta_3 = 0.2;$$

$$(\xi_{ij,\ell}|Y_i = 2) \sim t_{2\ell+2}(3), \ell = 1, 2, 3;$$

$$(\xi_{ij}|Y_i = 3) \sim \mathcal{N}((0, 0, 0)^\top, \text{diag}(1.2, 0.8, 0.4)).$$
 2D functional data are generated as Model III.

We chose to observe the 1D functional data on 15 evenly spaced grid points on  $[0, 1]$ . The number of features for 2D functional data, number of grid points  $m$ , and sample sizes  $n_k$  were chosen the same as

TABLE 4  
The average true classification rates for Models IV, V, and VI.

Model	Method	$n_k$	$m = 30$		$m = 60$		
			$p = 80$	$p = 130$	$p = 80$	$p = 130$	
IV	fB-DNN	100	<b>0.876</b>	<b>0.878</b>	<b>0.881</b>	<b>0.879</b>	
		200	0.912	<b>0.912</b>	0.911	0.911	
	f-DNN	100	0.881	0.877	0.880	0.879	
		200	<b>0.913</b>	0.910	<b>0.912</b>	<b>0.912</b>	
	mfDNN	100	0.302	0.301	0.290	0.301	
		200	0.308	0.303	0.313	0.303	
	f-SVM	100	0.397	0.370	0.390	0.364	
		200	0.573	0.475	0.560	0.464	
	f-kNN	100	0.867	0.868	0.867	0.868	
		200	0.911	0.903	0.911	0.903	
	V	fB-DNN	100	0.970	0.970	0.977	<b>0.978</b>
			200	<b>0.987</b>	<b>0.986</b>	<b>0.989</b>	0.979
f-DNN		100	<b>0.973</b>	<b>0.974</b>	<b>0.978</b>	0.973	
		200	0.985	0.986	0.985	<b>0.986</b>	
mfDNN		100	0.304	0.294	0.300	0.292	
		200	0.306	0.305	0.310	0.315	
f-SVM		100	0.319	0.315	0.319	0.316	
		200	0.356	0.342	0.354	0.340	
f-kNN		100	0.485	0.466	0.485	0.466	
		200	0.584	0.565	0.582	0.564	
VI		fB-DNN	100	<b>0.963</b>	<b>0.961</b>	<b>0.964</b>	<b>0.961</b>
			200	<b>0.966</b>	<b>0.968</b>	<b>0.978</b>	<b>0.966</b>
	f-DNN	100	0.961	0.932	0.959	0.946	
		200	0.961	0.948	0.967	0.965	
	mfDNN	100	0.291	0.301	0.302	0.289	
		200	0.310	0.315	0.308	0.310	
	f-SVM	100	0.458	0.402	0.451	0.392	
		200	0.651	0.485	0.637	0.467	
	f-kNN	100	0.957	0.954	0.958	0.954	
		200	0.964	0.962	0.964	0.961	

described in Section 4.1. The chosen optimal numbers of FPCs, hidden layers and neurons in each layer also followed the same setting in in Section 4.1. For each model, the number of total features  $p \in \{80, 130\}$ , accounting for both the 1D and 2D functional features. Table 3 shows the EMR and FP for Models IV to VI. Table 4 depicts their classification accuracy.

The proposed fB-DNN classifier consistently outperforms its counterparts across all mixture functional data scenarios. Specifically, in Model IV, when  $n = 100$ , the EMR of f-DNN is approximately one-fourth to one-third of fB-DNN's EMR; when  $n = 200$ , the EMR of f-DNN is only one-twentieth of fB-DNN's EMR. Notably, fB-DNN's FP is extremely smaller compared to that of f-DNN across all settings. This discrepancy suggests that f-DNN struggles to correctly discern important features. In contrast, our proposed fB-DNN efficiently extracts significant features from the continuum within the complex mixture functional data framework. Furthermore, fB-DNN demonstrates the ability to uncover underlying distributions of functional data clusters effectively. Similar to the 2D functional data cases, both f-DNN and fB-DNN exhibit comparable performance across all scenarios, while the classification accuracy of alternative methods is consistently one-half or less than one-third of fB-DNN's accuracy in Model V, suggesting the possible detrimental impact of retaining redundant features on classification performance. Once again, our proposed classifier demonstrates a distinct advantage over its competitors in addressing complex functional data classification challenges.

## 5. An application for Alzheimer's disease with brain scans

Brain scans, which can be considered as 2D or 3D functional data, play a pivotal role in the diagnosis of AD. Accurately identifying the affected regions while simultaneously excluding areas without pathology is crucial. This not only facilitates the development of targeted treatment strategies but also helps spare individuals from unnecessary procedures or therapies, ensuring that resources are aptly allocated. As an application, we used the dataset obtained from the ADNI database (<http://adni.loni.usc.edu>). The ADNI is a longitudinal multicenter study designed to develop clinical, imaging, genetic, and biochemical biomarkers for the early detection and tracking disease progression of AD. From this database, we included 79 patients in AD group, 45 patients in EMCI group, and 101 people in CN group whose PET data are available.

For AD group, patients' age ranges from 59 to 88, with an average age of 76.49; and there are 33 females and 46 males among these 79 subjects. For EMCI group, patients' age ranges from 57 to 89, with an average age of 72.33; and there are 26 females and 19 males among these 45 subjects. For CN group, patients' age ranges from 62 to 87, with an average age of 75.98; and there are 40 females and 61 males among these 101 subjects. We collected 10 1D functional data for each subject. These variables represent



TABLE 6  
Classification Accuracy and Selected Features of Different Models for ADNI Dataset.

Data	Model	Accuracy (%)	Selected features
2D	mfDNN	52.9%	—
	f-SVM	50.0%	—
	f-kNN	51.5%	—
	f-DNN	61.8%	Scans 16–29
	fB-DNN	<b>63.2%</b>	Scans 18–25
1D & 2D	mfDNN	61.8%	—
	f-SVM	51.5%	—
	f-kNN	58.8%	—
	f-DNN	63.2%	Biomarkers 2–10, Scan 61
	fB-DNN	<b>70.6%</b>	Biomarkers 2–9, Scans 15–35

time-based biomarkers, recorded from the start of each patient’s participation in the study, and the numbers of observations for each variable vary from 2 to 15. The variable names and their descriptions are listed in Table 5. Figure 1 depicts four functional biomarkers observed varying over 180 months. All 2D PET scans were reoriented into  $79 \times 95 \times 68$  voxels, which means that each patient has 68 sliced 2D images with  $79 \times 95$  pixels. This PET dataset has been post-processed.

TABLE 5  
Summary of Functional Biomarkers for Alzheimer’s Disease

Variable Name	Description
1. FDG	Fluorodeoxyglucose-PET measures for cerebral metabolic rates
2. CDRSB	Clinical Dementia Rating-Sum of Boxes
3. ADAS13	AD Assessment Scale-Cognitive Subscale (13 items)
4. ADASQ4	Delayed Word Recall Score
5. MMSE	Mini-Mental State Examination
6. RAVLT.learning	Rey Auditory Verbal Learning Test (learning score)
7. RAVLT.forgetting	Rey Auditory Verbal Learning Test (forgetting score)
8. LDELTOTAL	Logical Memory Delayed Recall (total score)
9. mPACCdigit	Modified Preclinical Alzheimer Cognitive Composite (digit symbol-coding)
10. mPACCtrailsB	Modified Preclinical Alzheimer Cognitive Composite (Trail Making Test Part B)

Given the complex and voluminous nature of the functional data, our objective is twofold: to provide physicians with insights into critical disease features and to construct a high-performance classifier for diagnosing the status of new patients. Implementation follows details in Section 3. Regarding input data, we consider classification based solely on the 2D imaging data, as well as datasets comprising a mixture of 1D functional data (time-based biomarkers) and 2D functional data (2D images). The classification and feature selection results are summarized in Table 6.

Clearly, all classifiers have improved classification accuracy when 1D functional data is included along with 2D functional data. This observation underscores the importance of leveraging complex multidimensional functional data. Both fB-DNN and f-DNN exhibit higher classification accuracy compared to alternative methods. When comparing fB-DNN and f-DNN, fB-DNN shows slightly better performance. However, f-DNN selects a questionable slice (#61) in the 1D & 2D setting. It is well known that Alzheimer’s disease

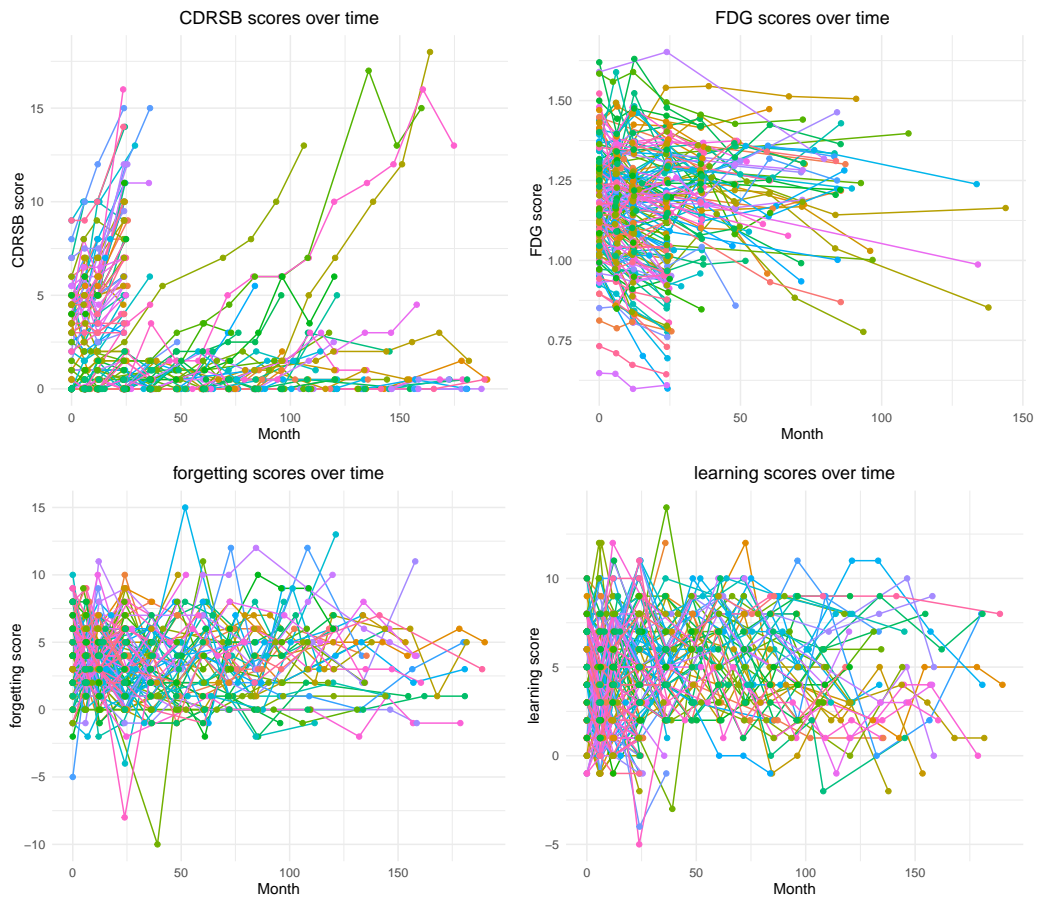


FIG 1. Four functional biomarkers from ADNI dataset for each subject. Top: Clinical Dementia Rating-Sum of Boxes (left) and Fluorodeoxyglucose-PET measures for cerebral metabolic rates (right). Bottom: Rey Auditory Verbal Learning Test learning score (left) and forgetting score (right).

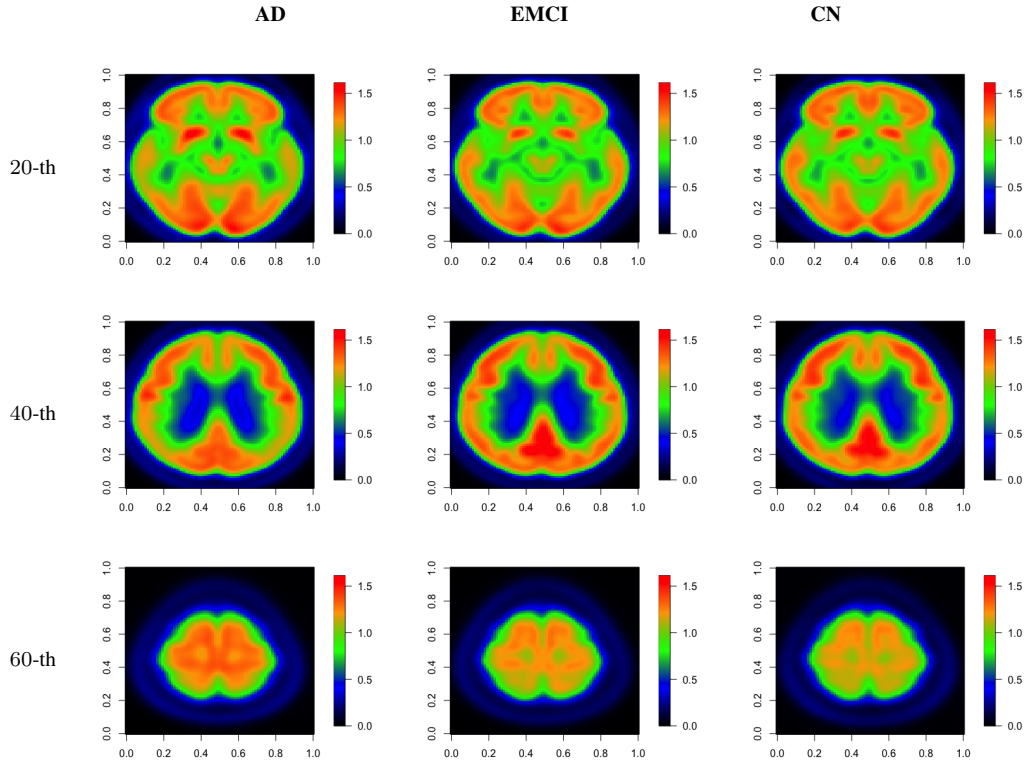


FIG 2. The 20-th, the 40-th and the 60-th slices of AD group (left column), EMCI group (middle column), and CN group (right column) from three random samples.

destroys neurons and their connections in the hippocampus, the entorhinal cortex, and the cerebral cortex. These regions correspond to the first 25 slices, as discussed in the real data analysis results by [17]. Notably, our proposed fB-DNN algorithm effectively selects reasonable and significant features, presenting promising findings for neurologists. The 2D slices and biomarkers identified by the algorithm offer valuable insights for distinguishing between CN, EMCI, and AD groups, guiding further medical evaluations targeted at these critical brain locations and biomarkers. Therefore, considering both classification and feature selection accuracy, fB-DNN stands out among existing classifiers.

## 6. Discussion

This paper introduces a novel method for performing classification of complex functional data using DNNs framework. The proposed fB-DNN algorithm establishes a relationship between a scalar outcome and a set of predictors through a DNN-based approach, enabling it to handle various factors and correlations between functions effectively. Additionally, it efficiently selects significant functional variables, thereby enhancing classification accuracy. Leveraging the principles of Lasso regularization, the method effectively manages large numbers of functional covariates and image data. Moreover, it demonstrates scalability to large datasets through automated coding, with potential for further flexibility in accommodating mixed

curved data and image data. Notably, this work represents the first unified framework for multiclassification and feature selection in the context of multidimensional functional data.

To the best of our knowledge, even for simple i.i.d. data, no existing work has addressed feature selection consistency for DNN that incorporate residual layers and penalty functions. This represents a challenging and promising direction for our future research in functional data classification.

## Acknowledgement

We thank an Associate Editor and two referees for their constructive comments which have helped to improve the presentation of the paper. We extend our gratitude to Sukruth Rao for his helpful assistance in preparing the Python codes. Cao's research was also partially supported by National Science Foundation under Grants DMS-2413301, CNS-2319342 and CNS-2319343.

Data used in preparation of this article were obtained from the Alzheimer's Disease Neuroimaging Initiative (ADNI) database (<http://adni.loni.usc.edu>). As such, the investigators within the ADNI contributed to the design and implementation of ADNI and/or provided data but did not participate in analysis or writing of this report. A complete listing of ADNI investigators can be found at: [http://adni.loni.usc.edu/wp-content/uploads/how\\_to\\_apply/ADNI\\_Acknowledgement\\_List.pdf](http://adni.loni.usc.edu/wp-content/uploads/how_to_apply/ADNI_Acknowledgement_List.pdf).

## 7. Appendix

In this Appendix, we provide Algorithm 3, assumptions, and additional computational time for numerical studies.

### 7.1. Algorithm 3

---

#### Algorithm 3 Updating $\mathbf{b}_j$ and $W_1^{(j)}$ in Model (2.7)

---

- 1: **Inputs:**  
hierarchy coefficient  $C$ , learning rate  $\alpha$ , network weights  $\mathbf{b}_j$  and  $W_j$ .
  - 2: Sort  $\text{vec}(W_1^{(j)}) \in \mathbb{R}^{\nu_j}$  and denote by  $|\omega_{j(1)}| \geq \dots \geq |\omega_{j(\nu_j)}|$ , where  $\nu_j = r_j q_2$
  - 3: **for**  $u = 0, \dots, \nu_j$  **do**
  - 4:     Calculate  $\zeta_{ju} = \frac{C}{1+C^2} S_{\alpha\lambda}(\|\mathbf{b}_j\| + C \sum_{v=1}^u |\omega_{j(v)}|)$ ,  $S_{\alpha\lambda}(z) = \text{sign}(z) \max(|z| - \alpha\lambda, 0)$ .
  - 5: **end for**
  - 6: Select  $u_j^*$  as the smallest integer from  $\{u : |\omega_{j(u)}| \geq \zeta_{ju} \geq |\omega_{j(u+1)}|\}$ , where  $\omega_{j(0)} = +\infty$ ,  $\omega_{j(\nu_j+1)} = 0$ .
  - 7: Update  $\mathbf{b}_j \leftarrow \frac{\zeta_{ju_j^*} \mathbf{b}_j}{C \|\mathbf{b}_j\|}$ .
  - 8: **for**  $k = 1, \dots, r_j$  **do**
  - 9:     **for**  $l = 1, \dots, q_2$  **do**
  - 10:         Update  $W_{1kl}^{(j)} \leftarrow \text{sign}(W_{1kl}^{(j)}) (\zeta_{ju_j^*} \wedge |W_{1kl}^{(j)}|)$
  - 11:     **end for**
  - 12: **end for**
  - 13: **Outputs:**  $\mathbf{b}_j$  and  $W_1^{(j)}$
-

## 7.2. Key assumptions

In the following, we provide the technical assumptions for Theorem 2.2. Let  $\boldsymbol{\xi}_{\mathcal{A}} = (\boldsymbol{\xi}_{j_1}, \boldsymbol{\xi}_{j_2}, \dots, \boldsymbol{\xi}_{j_{|\mathcal{A}|}})^\top$ , such that  $j_\ell \in \mathcal{A}$ , and  $\boldsymbol{\xi}_{\mathcal{A}}^{r_{\mathcal{A}}} = \left( \boldsymbol{\xi}_{j_1}^{(r_{j_1})}, \boldsymbol{\xi}_{j_2}^{(r_{j_2})}, \dots, \boldsymbol{\xi}_{j_{|\mathcal{A}|}}^{(r_{j_{|\mathcal{A}|}})} \right)^\top$ . By definition, the Bayes classifiers  $f_{0k}$  are functions of  $\boldsymbol{\xi}_{\mathcal{A}}$ , and denote the dimension of  $\boldsymbol{\xi}_{\mathcal{A}}^{r_{\mathcal{A}}}$  as  $r_{\mathcal{A}}$ .

**Assumption 3. (a)** *There exists universal constants  $c_2 > 0$  and  $M$ , such that  $\mathbb{P} \left( \frac{f_{01}(\boldsymbol{\xi}_{\mathcal{A}}) - f_{02}(\boldsymbol{\xi}_{\mathcal{A}})}{f_{01}(\boldsymbol{\xi}_{\mathcal{A}}) + f_{02}(\boldsymbol{\xi}_{\mathcal{A}})} \leq t \right) \leq c_1 t^M$ , for any  $t \in (0, 1]$ ;*

**(b)** *There exists a decreasing function  $D(\cdot) : [1, \infty) \rightarrow \mathbb{R}$ , and for some positive constants  $c_2, c_3$ ,  $\sup_{r \geq 1} r^{c_2} D(r) < \infty$  and  $\mathbb{E} \left( \left| \log \frac{f_{01}(\boldsymbol{\xi}_{\mathcal{A}})}{f_{02}(\boldsymbol{\xi}_{\mathcal{A}})} - \log \frac{f_1(\boldsymbol{\xi}_{\mathcal{A}}^{r_{\mathcal{A}}})}{f_2(\boldsymbol{\xi}_{\mathcal{A}}^{r_{\mathcal{A}}})} \right| \right) \leq c_3 D(r_{\mathcal{A}})$ ;*

**(c)**  *$L \asymp \log_2(n)$ ,  $\|\mathbf{q}\|_\infty \asymp (n \log^{-3} n)^{\frac{\alpha_1}{\alpha_1 + M + 2}}$ ,  $s \asymp n^{\frac{\alpha_1}{\alpha_1 + M + 2}} \log_2 n$ ,  $n^{\frac{M+1}{c_2(\alpha_1 + M + 2)}} \lesssim r_{\mathcal{A}} < \sum_{j=1}^p r_j \lesssim n^{\frac{\alpha_1}{\alpha_1 + M + 2}}$ ,  $\|\mathbf{W}\|_\infty \asymp (n \log^{-3} n)^{\min_u (\beta_u^*(M+2) + t_u)^{-1}}$ .*

**Assumption 4.** *For any  $k = 1, \dots, K$ ,*

**(a)** *There exists a universal constant  $c_2 > 0$  and a set of constants  $M_1, \dots, M_K > 0$ , such that for any  $t \in (0, 1]$ ,  $\mathbb{P}(f_{0k}(\boldsymbol{\xi}_{\mathcal{A}}) \leq t) \leq c_1 t^{M_k}$ .*

**(b)** *There exists a decreasing function  $D(\cdot) : [1, \infty) \rightarrow \mathbb{R}$  and positive constant  $c_2, c_3$ , with  $\sup_{r \geq 1} r^{c_2} D(r) < \infty$ , such that  $\mathbb{E}(|f_{0k}(\boldsymbol{\xi}_{\mathcal{A}}) - f_k(\boldsymbol{\xi}_{\mathcal{A}}^{r_{\mathcal{A}}})|) \leq c_3 D(r_{\mathcal{A}})$ ;*

**(c)**  *$L \asymp \log_2(n)$ ,  $\|\mathbf{q}\|_\infty \asymp n^{\frac{\alpha_2}{\alpha_2 + M_{\hat{k}} + 1}}$ ,  $s \asymp n^{\frac{\alpha_2}{\alpha_2 + M_{\hat{k}} + 1}} \log_2(n)$ ,  $n^{\frac{M_{\hat{k}} + 1}{c_2(\alpha_2 + M_{\hat{k}} + 1)}} \lesssim r_{\mathcal{A}} < \sum_{j=1}^p r_j \lesssim n^{\frac{\alpha_2}{\alpha_2 + M_{\hat{k}} + 1}}$ ;*

**(d)** *There exists a small constant  $c_4 > 0$ , such that  $\mathbb{P}(f_{0k}(\boldsymbol{\xi}_{\mathcal{A}}) > c_4) = 1$ .*

**Remark 1.** *Assumption 3 and Assumption 4 describe the necessary conditions for the fast convergence rate with respect to the Bayes classifier under binary and multi-class classification cases, respectively. Assumptions 3(a) and 4(a) control the decay rate of the  $f_{0k}$ , which is a typical assumption in classification convergence rates literature. Assumptions 3(b) and 4(b) provide the uniform upper bound for the difference of the expected difference of  $f_{0k}$  and  $f_k$ . Assumptions 3(c) and 4(c) provide the optimal neural network architecture with respect to the considered classification task. Assumption 4(d) indicates that the conditional probability should be bounded away from zero, which is a regular condition for multi-class classification problem [16].*

We define

$$\alpha_1^* = (1 + M) / (2 + M + \alpha_1) \quad \text{and} \quad \alpha_2^* = (1 + M_{\hat{k}}) / (1 + M_{\hat{k}} + \alpha_2). \quad (7.1)$$

TABLE 7  
The average computational time (in minutes) for Model I.

Method	$n_k$	$m = 30$		$m = 60$	
		$p = 50$	$p = 100$	$p = 50$	$p = 100$
fb-DNN	100	280.18	348.87	245.04	374.39
	200	290.74	432.24	304.46	382.51
f-DNN	100	90.02	94.33	90.83	91.79
	200	87.46	100.62	89.88	95.39
mfDNN	100	24.63	25.04	24.68	25.35
	200	25.46	25.98	25.62	26.14
f-SVM	100	0.14	0.15	0.15	0.15
	200	0.17	0.19	0.17	0.18
f-kNN	100	0.13	0.14	0.12	0.14
	200	0.16	0.18	0.14	0.19

### 7.3. Computational time

The computation job of this paper is conducted at Michigan State University high performance computing center, where each compute node containing multiple CPU cores and substantial memory (RAM). The specific hardware configurations may vary, but it always includes 1 CPU and 12 GB RAM as default for each replicates of the parallel computing.

The computing times for different models in the simulation settings are very similar to each other. Table 7 presents the average computational time (in minutes) for Model I. As expected, all DNN-based methods are computationally more expensive than the f-SVM and f-kNN methods. This can be attributed to several factors, including layer depth, model complexity, parameter volume, and memory requirements, as discussed in classic deep learning literature. Reducing the computational cost of the proposed fb-DNN method represents a promising direction for future research. Since fb-DNN performs both feature selection and classification simultaneously, it requires additional computational resources compared to f-DNN and mfDNN, which do not include a feature selection process.

### References

- [1] José R Berrendero, Antonio Cuevas, and José L Torrecilla. Variable selection in functional data classification: a maxima-hunting proposal. *Statistica Sinica*, 7(2):619–638, 2016.
- [2] F. C erou and A. Guyader. Nearest neighbor classification in infinite dimension. *ESAIM: Probability and Statistics*, 10:340–355, 2006.
- [3] Wenlin Dai and Marc G Genton. An outlyingness matrix for multivariate functional data classification. *Statistica Sinica*, 28(4):2435–2454, 2018.
- [4] Xiongtao Dai, Hans-Georg M uller, and Fang Yao. Optimal Bayes classifiers for functional data and density ratios. *Biometrika*, 104(3):545–560, 2017.

- [5] Aurore Delaigle and Peter Hall. Achieving near-perfect classification for functional data. *Journal of the Royal Statistical Society, Series B*, 74:267–286, 2012.
- [6] Aurore Delaigle and Peter Hall. Classification using censored functional data. *Journal of the American Statistical Association*, 108(504):1269–1283, 2013.
- [7] Kaiming He, Xiangyu Zhang, Shaoqing Ren, and Jian Sun. Deep residual learning for image recognition. In *Proceedings of the IEEE Conference on Computer Vision and Pattern Recognition*, pages 770–778, 2016.
- [8] G. M. James and T. Hastie. Functional linear discriminant analysis for irregularly sampled curves. *Journal of the Royal Statistical Society, Series B*, 63:533–550, 2001.
- [9] Ismael Lemhadri, Feng Ruan, Louis Abraham, and Robert Tibshirani. Lassonet: A neural network with feature sparsity. *Journal of Machine Learning Research*, 130:10–18, 2021.
- [10] Cai Li, Luo Xiao, and Sheng Luo. Joint model for survival and multivariate sparse functional data with application to a study of alzheimer’s disease. *Biometrics*, 78(2):435–447, 2022.
- [11] Hongzhou Lin and Stefanie Jegelka. Resnet with one-neuron hidden layers is a universal approximator. In *Advances in Neural Information Processing Systems*, pages 6169–6178, 2018.
- [12] Issam-Ali Moindjié, Sophie Dabo-Niang, and Cristian Preda. Classification of multivariate functional data on different domains with partial least squares approaches. *Statistics and Computing*, 34(5), 2024.
- [13] Hans-georg Müller. Functional modelling and classification of longitudinal data. *Scandinavian Journal of Statistics*, 32(2):223–240, 2005.
- [14] J. Schmidt-Hieber. Nonparametric regression using deep neural networks with relu activation function. *The Annals of Statistics*, 48(4):1875–1897, 2020.
- [15] Lan Wang, Yongdai Kim, and Runze Li. Calibrating non-convex penalized regression in ultra-high dimension. *The Annals of Statistics*, 41(5):2505–2536, 2013.
- [16] Shuoyang Wang and Guanqun Cao. Multiclass classification for multidimensional functional data through deep neural networks. *Electronic Journal of Statistics*, 18(1):1248–1292, 2024.
- [17] Shuoyang Wang, Guanqun Cao, and Zuofeng Shang. Deep neural network classifier for multidimensional functional data. *Scandinavian Journal of Statistics*, 50(4), 2023.
- [18] Shuoyang Wang, Yuan Huang, and Guanqun Cao. Review on functional data classification. *WIREs Computational Statistics*, 16(1), 2023.
- [19] Shuoyang Wang, Zuofeng Shang, Guanqun Cao, and S. Jun Liu. Optimal classification for functional data. *Statistica Sinica*, 34(3), 2023.
- [20] Xuejing Wang, Bin Nan, Ji Zhu, and Robert Koeppe. Regularized 3d functional regression for brain image data via haar wavelets. *The annals of applied statistics*, 8(2):1045, 2014.

- [21] Xuejing Wang, Bin Nan, Ji Zhu, Robert Koeppel, and Kirk Frey. Classification of adni pet images via regularized 3d functional data analysis. *Biostatistics & epidemiology*, 1(1):3–19, 2017.
- [22] Kaijie Xue, Jin Yang, and Fang Yao. Optimal linear discriminant analysis for high-dimensional functional data. *Journal of the American Statistical Association*, 2023.
- [23] Weichang Yu, Sara Wade, D. Howard Bondell, and Lamiae Azizi. Nonstationary gaussian process discriminant analysis with variable selection for high-dimensional functional data. *Journal of Computational and Graphical Statistics*, 32(2):588–600, 2023.